Hydrodynamic Modeling of Planing Boats with Asymmetry and Steady Condition.

R. Algarín. & O. Tascón
Cotecmar, Cartagena, Colombia

ABSTRACT: This paper shows a hydrodynamic study of planing crafts, monohull type with hard chine, sailing in asymmetry and steady condition with added trim and roll. For this, the flow potential theory of Wagner (1932) is extended for the 2D impact including the asymmetric entry with sections with knuckle, to obtain an analytic solution to calculate the pressure distribution in the boat. To transform the results to 3D, the slender body theory is applied to obtain the pressure distribution in the hull, in order to get the sway force, lift force, roll momentum, trim momentum and yaw momentum in the craft. The formulation is programed in Matlab© and the calculations are performed with low computational resources. The results obtained are compared with the experimental data of towing test of Brown & Klosinsky (1994) and simulations with the commercial software CFD Star –CMM+ © showing good agreement.

1. INTRODUCTION

Wagner (1932) developed an analytic formulation based on the flow potential theory and energy conservation to determine the pressure distribution during the 2D impact with symmetry entry. His results show:

$$\varphi = -w\sqrt{c^2 - y^2} \tag{1}$$

where φ is the potential function that describes the flow around the section, w is the vertical impact velocity, y is the horizontal axis, c is the half wetted beam as is shown in the figure 1, furthermore b is the beam of the section, d is the distance keel- chine, z is the vertical axis and β is the dead rise angle.

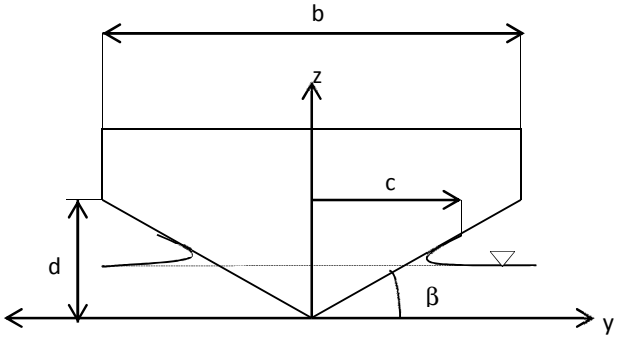

Figure 1. Wedge section with symmetry entry

The pressure distribution can be evaluated as:

$$\frac{P}{\rho} = -\dot{w}\sqrt{c^2 - y^2} + \frac{wc\dot{c}}{\sqrt{c^2 - y^2}} - \frac{w^2}{2}\frac{y^2}{c^2 - y^2} \tag{2}$$

Where P is the pressure and ρ is the flow density. In the case of a wedge the rate of the half beam is $\dot{c} = \frac{\pi}{2}\frac{w}{tan\beta}$

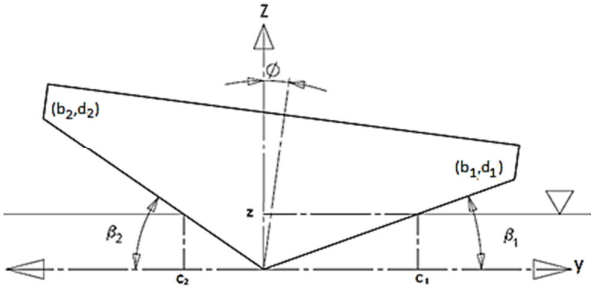

Figure 2. Wedge section with asymmetric entry

Toyama (1993) extended the model of Wagner (1932) for the asymmetric entry his results show:

$$\frac{P(\varsigma)}{\rho} = \dot{w}\, c\sqrt{1-\varsigma^2} + \frac{w\,\dot{c}(1+\mu\varsigma)}{\sqrt{1-\varsigma^2}} - \frac{w^2}{2}\frac{\varsigma^2}{1-\varsigma^2}, \tag{3}$$

Where $\varsigma = (y - \mu c)/c$, where μ is an asymmetric parameter defined as:

$$\mu = \begin{Bmatrix} f(T)(T-1)/(T+1), T \geq 1 \\ f(1/T)(T-1)/(T+1), T < 1 \end{Bmatrix} \tag{4}$$

Where $T=tg\beta_2/ tg\beta_1$

$$f(T) = \begin{Bmatrix} 0.77975 + 0.03371T + 0.001876T^2, 1 \leq T > 3 \\ 0.76773 + 0.015024T + 0.000539T^2, 3 \leq T < 10 \\ 0.80497 + 0.007208T + 0.000130T^2, 10 \leq T < 20 \end{Bmatrix} \tag{5}$$

$$\dot{c} = \frac{\pi T w}{(T+1)^2(1-\mu^2)\sqrt{1-\mu^2}} \left(\frac{1}{\tan(\beta_1)} - \frac{1}{\tan(\beta_2)} \right) \tag{6}$$

2. Model of asymmetric entry

The figure 2 shows a wedge section with asymmetry entry where β_1, β_2, c_1 y c_2 are the dead rise angle and the half beam in the sides 1 and 2 respectively. For the asymmetric entry the mean half beam and its rate is calculated as:

$$c = \frac{1}{2}(c_1 + c_2) \tag{7}$$

$$\dot{c} = \frac{1}{2}(\dot{c}_1 + \dot{c}_2) \tag{8}$$

Toyama (1993) introduced μ as asymmetric parameter but in the current model this parameter is evaluated as:

$$\mu = \frac{1}{2}(c_1 - c_2) \tag{9}$$

$$\dot{\mu} = \frac{1}{2}(\dot{c}_1 - \dot{c}_2) \tag{10}$$

The potential function proposed for the asymmetric entry is:

$$\varphi = -w\sqrt{c^2 - (-\mu + y)^2} \tag{11}$$

The potential function was derived respect to time and space and replacing in energy equation was obtained the pressure distribution for the asymmetric entry in the follow way:

$$\frac{P}{\rho} = -\dot{w}\sqrt{c^2 - (-\mu + y)^2} + \frac{w(c\dot{c} + (-\mu + y)\dot{\mu})}{\sqrt{c^2 - (-\mu + y)^2}} - \frac{w^2}{2}\frac{(-\mu + y)^2}{c^2 - (-\mu + y)^2} \tag{12}$$

For a wedge section is assuming that the asymmetric does not affect the jet velocity, the mean half beam and its rate are approximated with:

$$c = \frac{\pi}{4} wt \left(\frac{1}{tan(\beta_1)} + \frac{1}{tan(\beta_2)} \right) \tag{13}$$

$$\dot{c} = \frac{\pi}{4} w \left(\frac{1}{tan(\beta_1)} + \frac{1}{tan(\beta_2)} \right) \tag{14}$$

The asymmetry parameter is calculated as:

$$\mu = \frac{\pi}{4} wt \left(\frac{1}{tan(\beta_1)} - \frac{1}{tan(\beta_2)} \right) \tag{15}$$

$$\dot{\mu} = \frac{\pi}{4} w \left(\frac{1}{tan(\beta_1)} - \frac{1}{tan(\beta_2)} \right) \tag{16}$$

2.1 Flow separation from the knuckle

The boundary condition for the flow separation from the knuckle in the side 1 is P=0 in $y=b_1$ assuming constant velocity entry and replacing in the equation 12:

$$\frac{P}{\rho} = \frac{w(c\dot{c} + (-\mu + b_1)\dot{\mu})}{\sqrt{c^2 - (-\mu + b_1)^2}} - \frac{w^2}{2}\frac{(-\mu + b_1)^2}{c^2 - (-\mu + b_1)^2} = 0 \tag{17}$$

By simplifying the equation 17:

$$\frac{2(c\dot{c} + (-\mu + b_1)\dot{\mu})\sqrt{c^2 - (-\mu + b_1)^2}}{(-\mu + b_1)^2} = w \tag{18}$$

By integrating the equation 18

$$\frac{2}{3}\frac{[c^2 - (-\mu + b_1)^2]^{3/2}}{(-\mu + b_1)^2} - 2\sqrt{c^2 - (-\mu + b_1)^2} + 2cln\left| \frac{c + \sqrt{c^2 - (-\mu + b_1)^2}}{(-\mu + b_1)} \right| = w(t - t_1) \tag{19}$$

Where t_1 is the instant when the flow separation from the side 1 occurs. On another hand from the equations 7, 8, 9 y 10:

$$c_2 + \mu = c \tag{20}$$

$$\dot{c}_2 + \dot{\mu} = \dot{c} \tag{21}$$

Assuming that the flow separation from the knuckle in the side 1 does not affect the value of the half beam in the side 2:

$$c_2 = \frac{\pi}{2}\frac{wt}{tan\beta_2} \tag{22}$$

$$\dot{c}_2 = \frac{\pi}{2}\frac{w}{tan\beta_2} \tag{23}$$

The equations 19, 20 and 22 are solved iteratively to calculate c and μ. The equations 18, 21 and 23 are resolved to obtain $\dot{c}$ and $\dot{\mu}$, the pressure distribution is evaluated with the equation 12. When occurs the flow separation from the side 2 the boundary condition is P=0 en y=b_2.

$$\frac{P}{\rho} = \frac{w(c\dot{c} + (-\mu - b_2)\dot{\mu})}{\sqrt{c^2 - (-\mu - b_2)^2}} - \frac{w^2}{2}\frac{(-\mu - b_2)^2}{c^2 - (-\mu - b_2)^2} = 0 \tag{24}$$

By simplifying 24

$$\frac{2(c\dot{c} + (-\mu - b_2)\dot{\mu})\sqrt{c^2 - (-\mu - b_2)^2}}{(-\mu - b_2)^2} = w \tag{25}$$

By integrating the equation 25 is obtained:

$$\frac{2}{3}\frac{[c^2 - (-\mu - b_2)^2]^{3/2}}{(-\mu - b_2)^2} - 2\sqrt{c^2 - (-\mu - b_2)^2} + 2cln\left|\frac{c + \sqrt{c^2 - (-\mu - b_2)^2}}{(-\mu - b_2)}\right| = w(t - t_2) \tag{26}$$

Where t_2 is the instant when the flow separation from the side 2 occurs. When the flow separation occurs in both sides the equations 19 y 26 are solving to calculate c and μ, and $\dot{c}$ and $\dot{\mu}$ are obtained resolving 18 y 25.

3. RESULTS

The results obtained solving the actual model was compared with other authors in different conditions.

3.1 Symmetric entry

The figures 3 and 4 show the results of pressure distribution and force in the time for different wedges, the adimensional coefficients of pressure, force, moment and time are calculated as:

$$c_p = \frac{P}{\frac{1}{2}\rho w^2} \tag{27}$$

$$c_F = \frac{F}{\frac{1}{2}\rho b w^2} \tag{28}$$

$$c_M = \frac{M}{\frac{1}{2}\rho b^2 w^2} \tag{29}$$

$$\tau = \frac{wt}{\frac{1}{2}b} \tag{30}$$

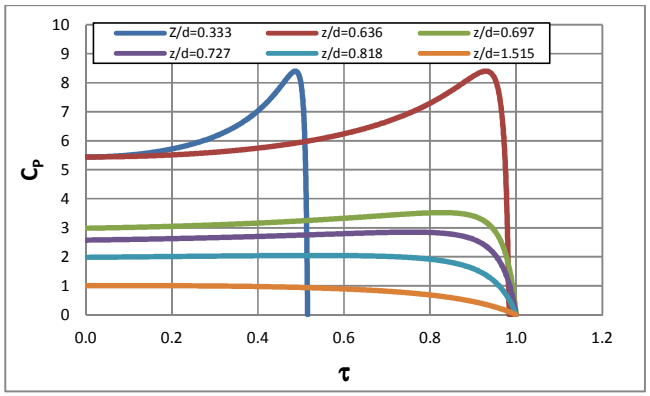

Figure 3. Pressure distribution in the time in a wedge with β=30°

In the figure 3 is noted a different behavior before and after the flow separation from the knuckle respect to the pressure distribution, before the flow separation the pressure is lower in the keel and increase when moving away from the keel, after the flow separation the pressure decrease with the time and the pressure is higher in the keel and decrease moving away from the keel.

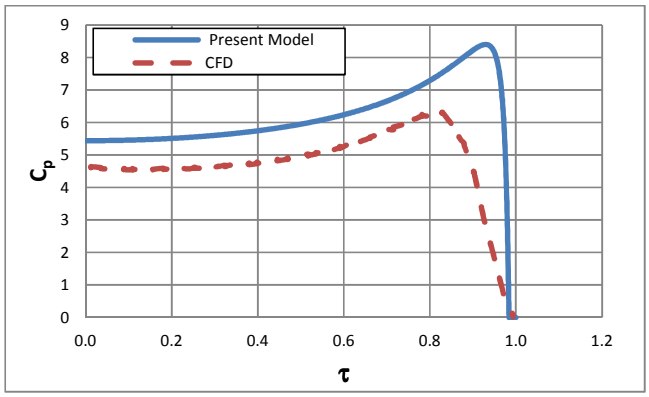

Figure 4. Pressure distribution z/d=0.636, β=30°

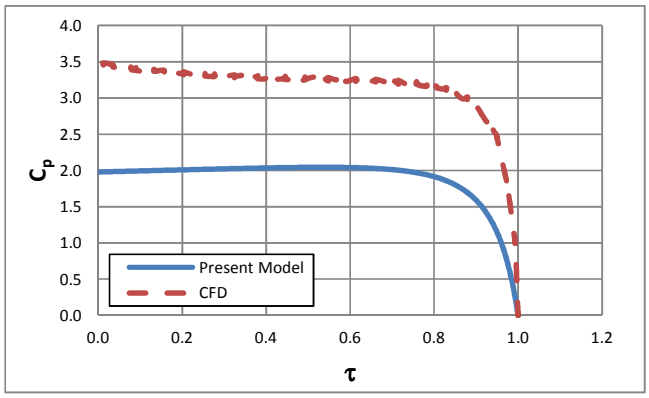

Figure 5. Pressure distribution z/d=0. 818, β=30°

The figures 4 and 5 show the results of pressure distribution before and after the flow separation from the knuckle, the values are compared with CFD simulation with the commercial software Star-CCM+©, the pressure obtained after the flow separation with CFD is higher than the results of the model. The figure 6, 7 and 8 shows the force during the impact for different wedges, the force was calculated of the integral of pressure distribution in the section. The force growth in a lineal way before the flow separation, after the separation the hydrodynamic force decrease as is shown in the figure, the results are compared with Tveitnes (2001) obtained a good agreement.

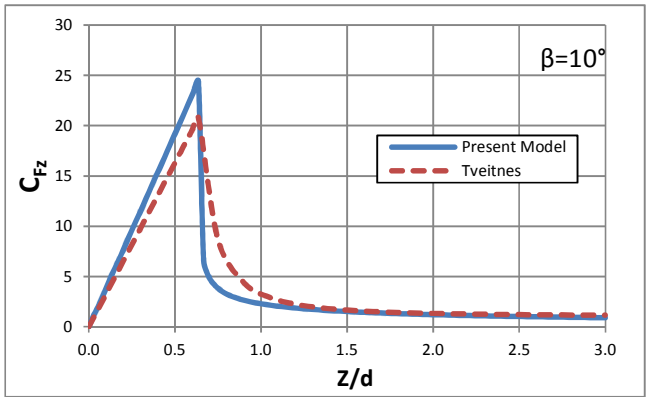

Figure 6. C_F vs z/d, β=10°

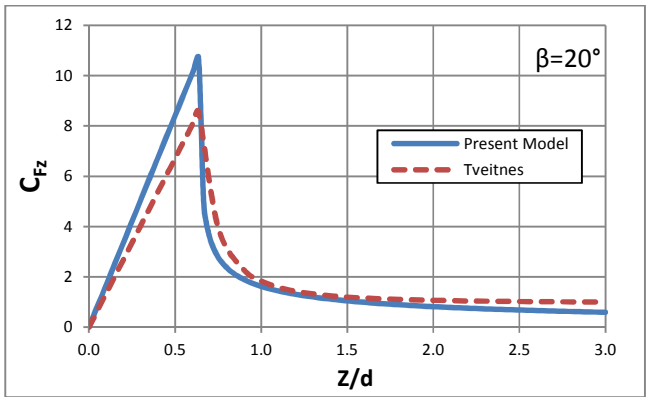

Figure 7. C_F vs z/d, β=20°

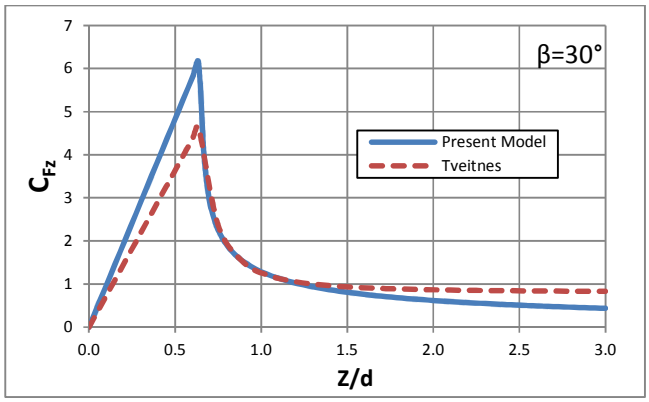

Figure 8 C_F vs z/d, β=30°

The Figure 9 and 10 show the results of the vertical force and peak pressure in the impact before the flow separation from the knuckle. The data are compared with Zhao & Faltinsen (1993), when the dead rise angle increase the pressure and force decrease in the impact.

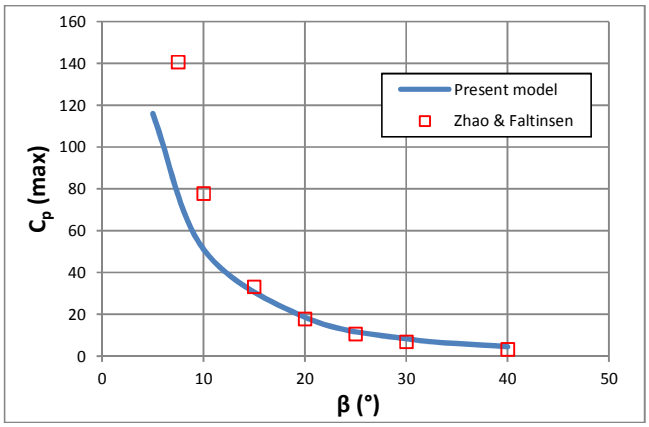

Figure 9. C_p vs β

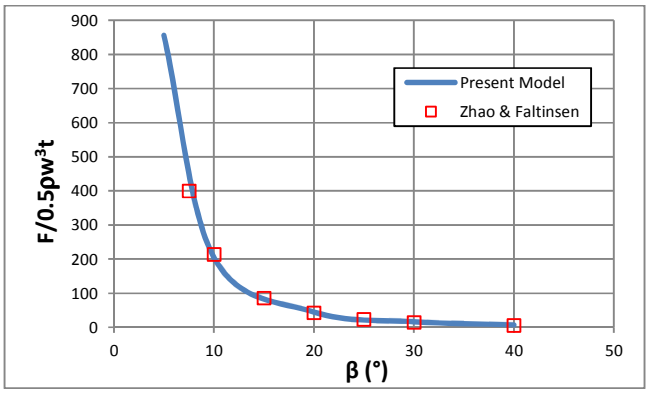

Figure 10. F_z vs β

3.2 Asymmetric entry

The figure 11 shows the pressure distribution in the time found with the model for a wedge with β_1=10° y β_2=30°. The results show that in the first instants of the impact the pressure is higher in the side 1, after de flow separation from this side the pressure begin to decrease and is higher in the side 2, after the flow separation from the side 2 the pressure continue decreasing y both sides of the section.

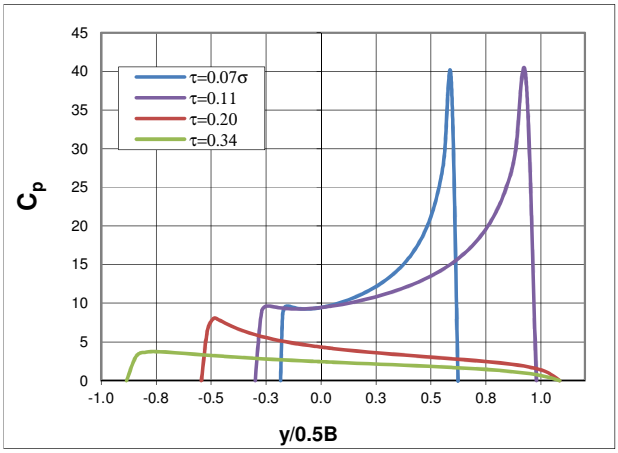

Figure 11. Pressure distribution during the impact, wedge with β_1=10° y β_2=30°

The figure 12 shows the pressure distribution before flow separation from the knuckle in the side 1, the results are compared with Toyama (1993) and CFD modeling. The figure 13 y 14 show the pressure distribution before and after the flow separation from the knuckle in the side 2 respectively, the data are compared with CFD simulations. The results obtained with CFD are higher after the flow separation in the side 2.

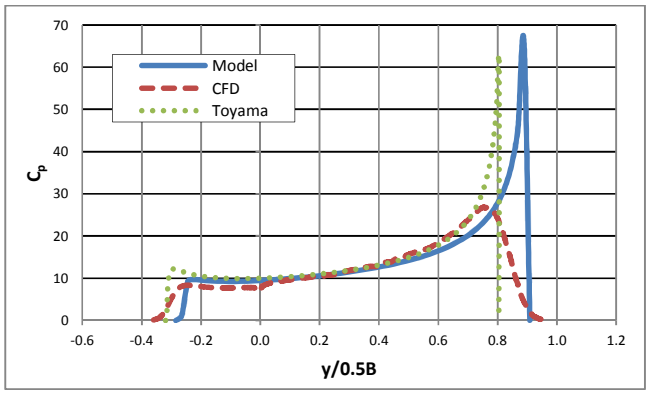

Figure 12. Pressure distribution τ=0.1, β_1=10° y β_2=30°

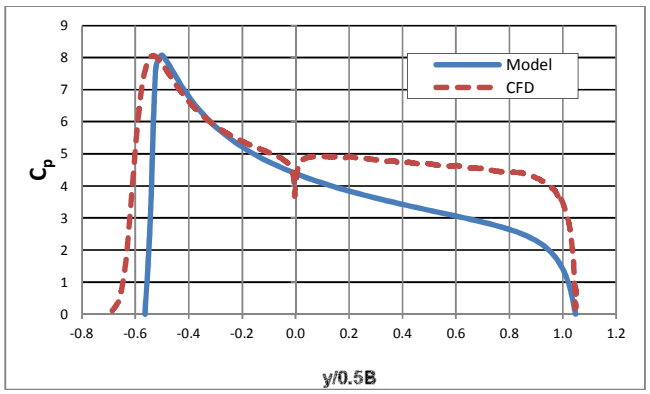

Figure 13. Pressure distribution τ=0.2, β_1=10° y β_2=30°

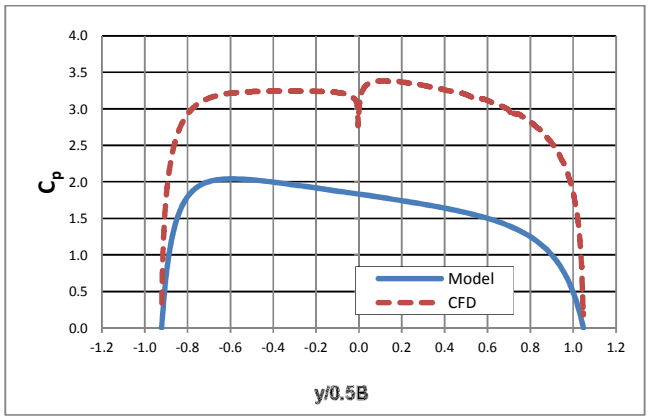

Figure 14. Pressure distribution τ=0.4, β_1=10° y β_2=30°

The horizontal force, vertical force and roll moment are calculated with the pressure integration in the section through the equations:

$$f_y = \int \hat{n}_y p dz \tag{31}$$

$$f_z = \int \hat{n}_z p dy \tag{32}$$

$$m_x = \int \hat{n} l p dl \tag{33}$$

The figures 15 and 16 show the variation in the time of the vertical force, and roll momentum during the impact for a wedge section with β_1=20° y β_2=30°, the results are compared with CFD modeling and Xu et al (1998), the current model show a good agreement with the other authors.

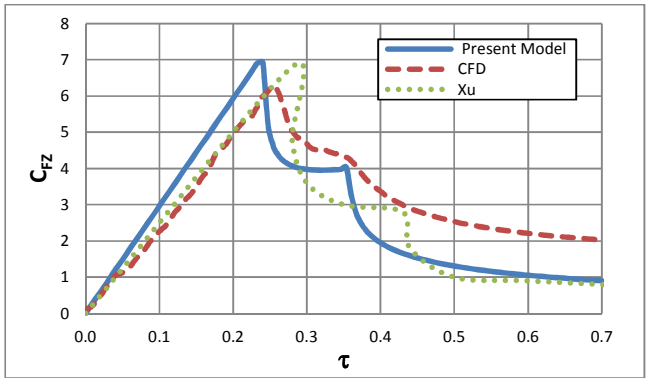

Figure 15. Vertical force variation during the impact, β_1=20° y β_2=30°

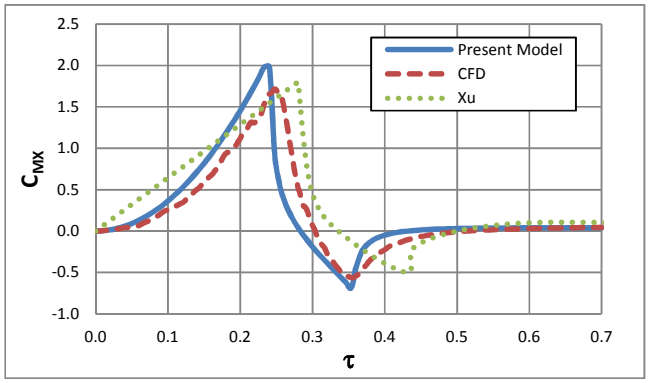

Figure 16. Roll moment variation during the impact, β_1=20° y β_2=30°

The figures 17, 18 and 19 show the variation in the time of the vertical force, horizontal force and roll momentum during the impact for a wedge section with β_1=10° y β_2=30°, the results are compared with CFD, the results of the model are very close to the simulation.

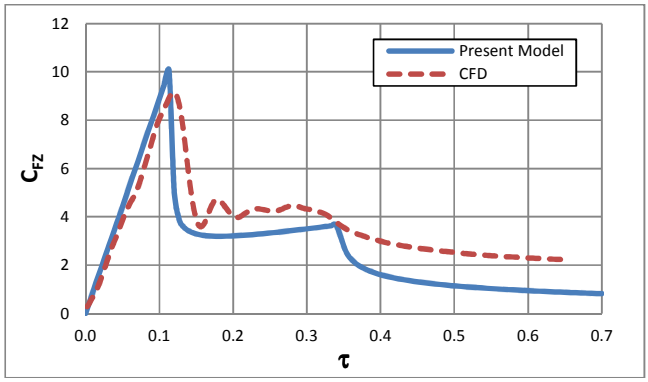

Figure 17. Vertical force variation during the impact, β_1=10° y β_2=30°

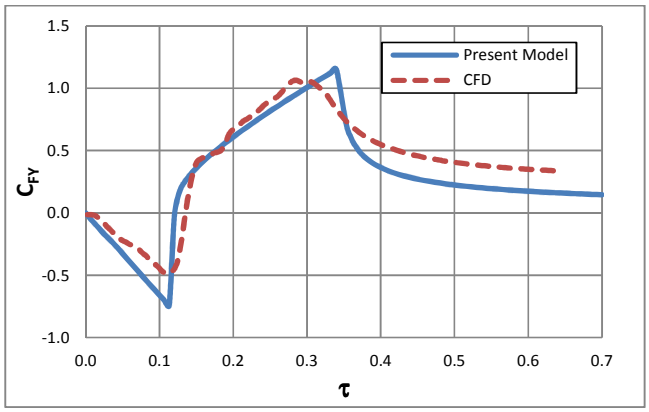

Figure 18. Horizontal force variation during the impact, β_1=10° y β_2=30°

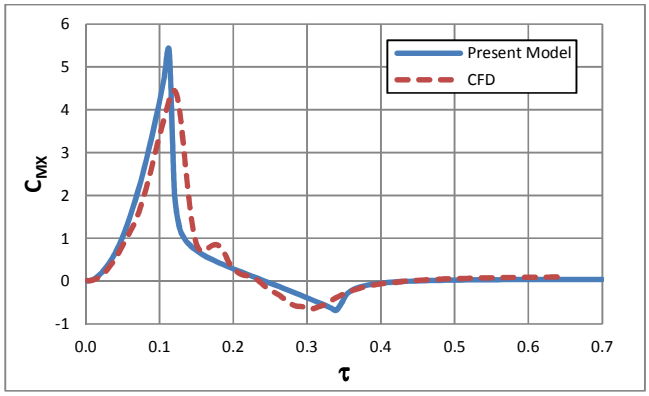

Figure 19. Roll moment variation during the impact, β_1=10° y β_2=30°

3.3 Flow separation from the keel

The critical conditions for the flow separation from the keel are evaluated, the boundary condition in this case is P=0 in y=0, applying in the equation 12:

$$\frac{P}{\rho} = \frac{w(c\dot{c} - \mu\dot{\mu})}{\sqrt{c^2 - \mu^2}} - \frac{w^2}{2}\frac{\mu^2}{c^2 - \mu^2} = 0 \tag{34}$$

To found the critical value was fixed β_1 and was changing the value of β_2 to satisfy the equation 34 in an iterative way. The figure 20 shows the results of the critical conditions, the results are compared with CFD simulation and Xu et al (1998). When the angle β_1 increase is required a higher value of β_2 for the flow separation.

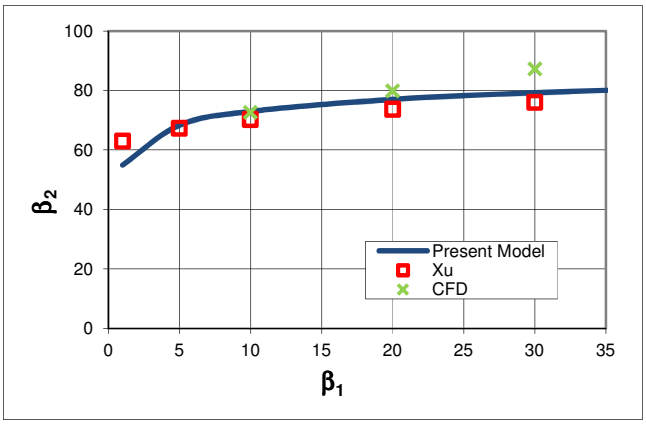

Figure 12. β_2 vs β_1, Critical condition for the flow separation from the keel

4. EXTENSION TO 3D

To extend the results to 3D is applied the slender body theory. The coordinate system used is shown in the figure 21, the origin is in the intersection of the keel line and aft, the *x* axis is parallel to the keel, the axes *y* and *z* correspond to the coordinates horizontal and vertical respectively.

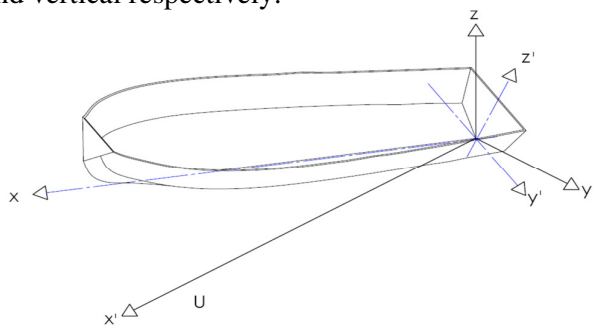

Figure 21. Coordinate system

The analysis were carry out programing an algorithm in matlab© that allows automate the calculations of the different variables. The forces and moments are calculated as:

$$F_y = \int f_y dx \tag{35}$$

$$F_z = \int f_z dx \tag{36}$$

$$M_x = \int m_x dx \tag{37}$$

$$M_y = \int x f_z dx \tag{39}$$

$$M_z = \int x f_y dx \tag{40}$$

Where F_y, F_z are the horizontal force and vertical force, M_x, M_y y M_z are the roll moment, trim moment and yaw momentum. The figures 22 to 25 show the results of pressure distribution, force and moment in a prismatic boat with beam B=2.6m, and dead rise angle β=22°, the equilibrium conditions are: a draft D=0.5m, trim angle θ=3°and roll angle ϕ=5°. In the figures 13 to 15 show the behavior of the forces in the boat, which depends on immersion of each section, the figures do not show the hydrostatic forces.

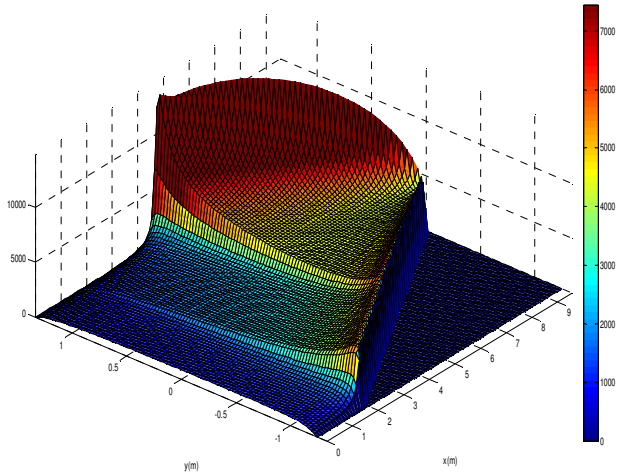

Figure 22. Pressure distribution in the hull (pa) β=22°, θ=3, ϕ=5 and D=0.5m

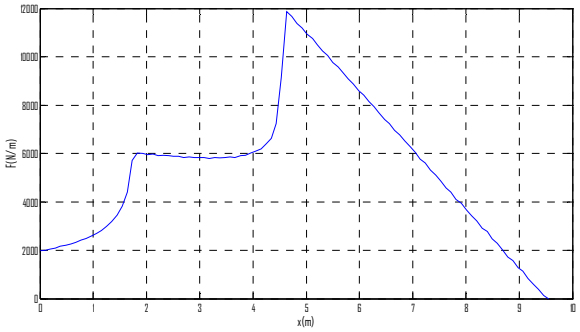

Figure 23. Vertical force distribution

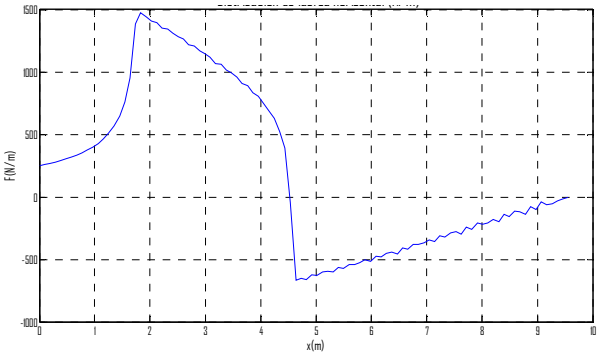

Figure 24. Horizontal force distribution

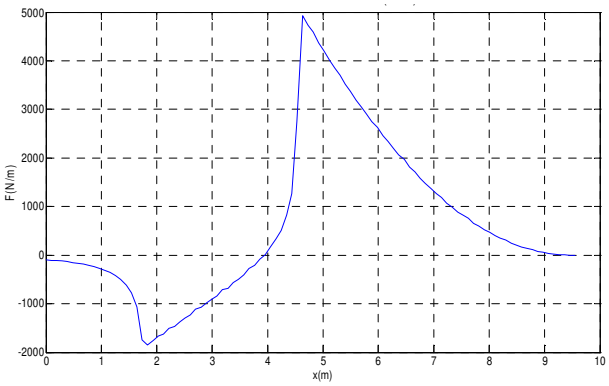

Figure 25. Roll moment distribution

The results obtained are compared with Brown & Klosinsky (1994), for a boat with β=20°, the values are shown in the table 2 and 3. The results are plotted in the figures 26 to 30. For this case the hydrostatic effect is included. The data show a minimum error of 4.4%, a maximum of 43% and an average of 5.7% respect to Brown & Klosinsky (1994). The coefficients of total force in hull are evaluated as:

$$C_y = \frac{F_y}{\frac{1}{2}\rho U^2 B_c^2} \quad (41)$$

$$C_z = \frac{F_z}{\frac{1}{2}\rho U^2 B_c^2} \quad (42)$$

$$C_{MX} = \frac{M_x}{\frac{1}{2}\rho U^2 B_c^3} \quad (43)$$

$$C_{MY} = \frac{M_y}{\frac{1}{2}\rho U^2 B_c^3} \quad (44)$$

$$C_{MZ} = \frac{M_z}{\frac{1}{2}\rho U^2 B_c^3} \quad (45)$$

Condition	τ (°)	ϕ (°)	ψ (°)	draft /B_c	F_{nb}
1	6	10	0	0,233	3
2	6	0	0	0,219	3
3	6	-10	0	0,275	3
4	6	10	0	0,146	4
5	6	0	0	0,142	4
6	6	-10	0	0,144	4

Table1. Conditions of Brown & Klosinsky (1994)

	C_y			C_z		
Condition	Actual	Exp	Error (%)	Actual	Exp	Error (%)
1	0.0098	0,0110	-10.9	0.1109	0,0980	13.2
2	0.0000	0,0007	--	0.1100	0,0983	11.9
3	-0.0096	-0,0092	4.4	0.1075	0,0982	9.5
4	0.0085	0,0090	5.6	0.0667	0,0547	21.9
5	0.0000	0,0008	--	0.0791	0,0552	43.1
6	-0.0087	-0,0076	14.7	0.0662	0,0549	20.6

Table 2. Forces results

	C_{MX}			C_{MY}			C_{MZ}		
	Actual	Exp	Error (%)	Actual	Exp	Error (%)	Actual	Exp	Error (%)
1	0.0100	0,0096	4.17	0.1240	0,133	-6.7	0.0166	0,0208	-20.2
2	0.0000	0,0009	--	0.1141	0,121	5.7	0.0000	0,0027	--
3	-0.0098	-0,0065	20.9	0.1161	0,1121	-10.9	-0.0159	-0,0142	8.16
4	0.0080	0,0074	8.1	0.0471	0,052	-10.2	0.0088	0,0111	20.7
5	0.0000	0,0005	--	0.0433	0,041	6.1	0.0000	0,0027	--
6	-0.0081	-0,0073	10.9	0.0459	0,0502	-9.2	-0.0088	-0,0068	29.4

Table3. Moment results

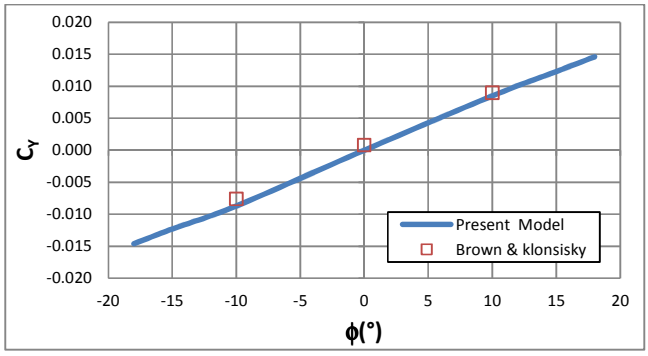

Figure 26. C_Y vs ϕ, C_v=4

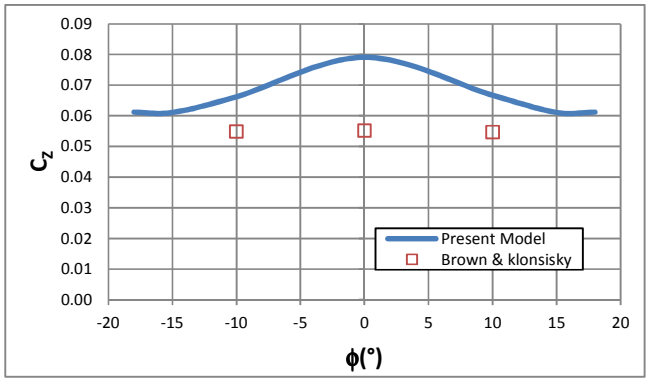

Figure 27. C_Z vs ϕ, C_v=4

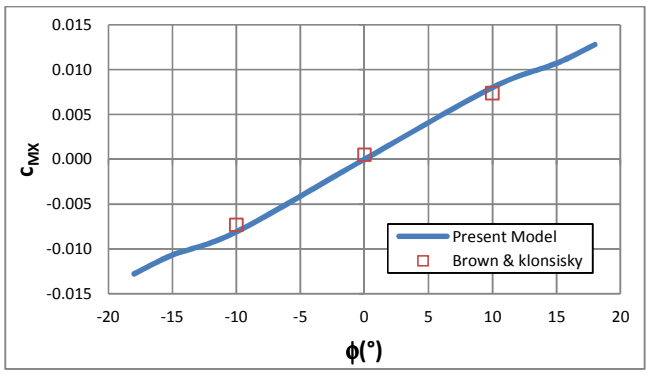

Figure 28. C_{MX} vs ϕ, C_v=4

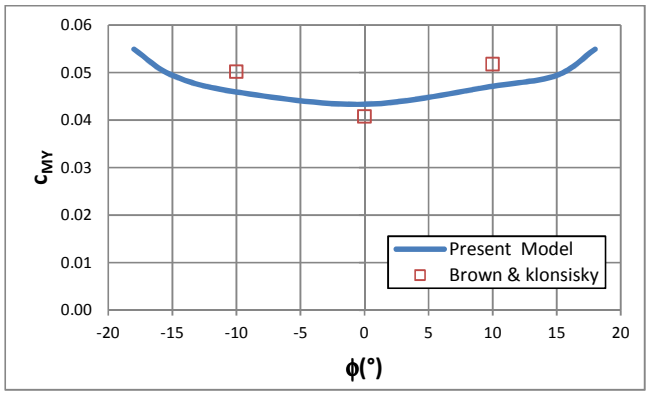

Figure 29. C_{MY} vs ϕ, C_v=4

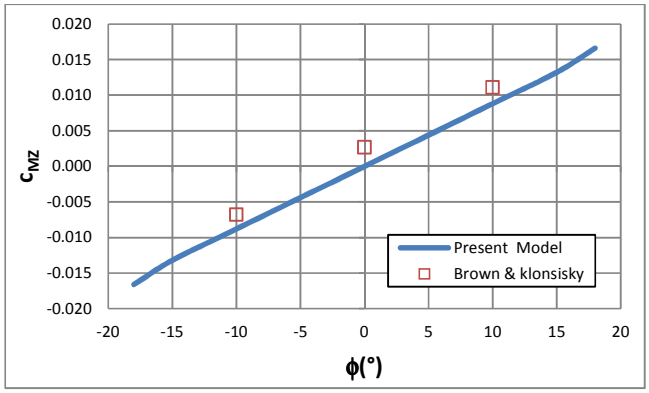

Figure 30. C_{MZ} vs ϕ, C_v=4

5. CONCLUSIONS

The model of Wagner (1932) was extended to the asymmetry entry for section with knuckle. The results show a good agreement respect to Tveitnes (2001), Zhao & Faltinsen (1993), Toyama (1993), Xu et al (1998) and CFD simulations. The formulation was extend to 3D by the application of SBT, the results are compared with experimental data of Brown & Klosinsky (1994).

REFERENCES

Algarin, R (2010). *Modelamiento del Impacto en Dos Dimensiones de Secciones Asimétricas con velocidad Horizontal con Aplicaciones en el Diseño de Botes de Planeo. [M.Sc. Thesis].* Barranquilla: Universidad del Norte. Programa de ingeniería Mecánica, 120p.

Brown, P. *and Klosinski W. (*1994) *Directional Stability Tests' of a 30 Degree Deadrise Prismatic Planing Hull.* USGC Report No. CG-D-27-94.

Caponetto, M., y SÖDING, H. (2003) *Motion Simulations for planing Boats in waves.* Ship technology research, Vol. 50, p 182-198.

Savander, Brant R. (1997) *Planing Hull steady Hydrodinamics [Ph.D Tesis].* Michigan: University of Michigan. Department of naval architecture and ocean engineering, 172p.

Tascón O. (2009) et al. *Numerical Computation of the Hydrodynamic Forces Acting on a Maneuvering Planing Hull Via Slender Body Theory - SBT and 2-D Impact Theory*, 10th International Conference on Fast Sea Transportation FAST 2009, Athens, Greece.

Tveitnes, *T. (*2001) *Application of Added Mass theory in planing [Ph.D. Thesis].* Glasgow: University of Glasgow. Department of naval architecture and ocean engineering, 339p.

Toyama Y. (1993) T*wo –dimensional water impact of unsymmetrical bodies.* Journal of Soc. Naval Arch. Japan. 1993, vol 173, p. 285-291.

Wagner, H. (1932) *Über stoss – und Gleitvorgänge and der Oberfläshe von Flüssigkeiten. En: Zeitschrift für Angewandte Mathematik und Mechanik. August,* 1932, vol 12, no 4, p. 193-215.

Xu, G.D. (2008). *Numerical simulation of oblique water entry of an asymmetrical wedge.* Journal of Ocean Engineering. August, 2008, vol 35, p. 1597-1603.

Xu, L., Troesch, A. and Vorus, W.S. *(*1998) *Asymmetric Vessel Impact and Planing Hydrodynamics.* Journal of Ship Research, September, 1998, vol 42, no 3, p. 187-198.

Zhao, R, L*. and Faltinsen, O.* (1993) *Water Entry of Two Dimensional Bodies.* Journal of fluid Mechanic, 1993, vol 246, p. 593-612.